Astron. Astrophys. 284, 331–339 (1994)

ASTRONOMY AND ASTROPHYSICS

An updated list of radio flux density calibrators

M. Ott[1], A. Witzel[1], A. Quirrenbach[2], T.P. Krichbaum[1], K.J. Standke[1], C.J. Schalinski[3], and C.A. Hummel[2]

[1] Max-Planck-Institut für Radioastronomie, Auf dem Hügel 69, D-53121 Bonn, Germany
[2] NRL/USNO Optical Interferometer Project, U.S. Naval Observatory, 3450 Mass. Ave. NW, Washington, DC 20392-5420, USA
[3] Institut de Radioastronomie Millimétrique, 300 rue de la Piscine, Domaine Universitaire, F-38406 St Martin d'Hères Cedex, France

Received 20 March 1993 / Accepted 20 June 1993

Abstract. We present new flux densities in the range 0.7 cm $\leq \lambda \leq$ 21 cm for the radio sources in the calibrator list of Baars et al. (1977). Most of these sources show significant variability on the time scale of a decade, with the notable exception of 3C286 and 3C295. We use these sources to link our relative measurements to the absolute scale of Baars et al.; for the other sources we present updated spectra. We assess the suitability of the individual sources for use as flux density calibrators.

Key words: observational methods – radio continuum: general

1. Introduction

The standard radio flux density scale is realized in a two-step process: first, the absolute flux density of a few primary calibrators is determined with an antenna whose efficiency can be calculated from first principles. Afterwards, a set of secondary calibrators is established by comparison with the primary standards. These calibrators should be strong, unresolved by the telescopes under consideration, non-variable, and distributed over the whole sky. Flux density measurements of arbitrary sources then can be referred to this set of secondary calibrators.

The absolute spectrum of Cas A and other primary standards was measured during the 1960's (e.g. Findlay 1966; Kellermann et al. 1969). The list of secondary calibrators with spectra based on the absolute spectrum of Cas A published by Baars et al. (1977; hereafter BGPW) has been widely used during the last 15 years.

However, several authors have pointed out deficiencies of the BGPW list (e.g. Turegano & Klein 1980, 3.5 cm; Moiseev & Nesterov 1985, 1.3 and 0.8 cm; Riley 1988, 73 cm; Ivanov & Stankevich 1989). Some of the problems encountered at short wavelengths are probably due to extrapolations of the source spectra in BGPW, which were based on measurements at $\lambda \geq 2.0$ cm. Another problem is variability of the sources in the BGPW list on the time scale of years to decades. For instance, the flux density ratio of 3C48 and NGC7027 at λ =2.8 cm has been observed to differ by up to 11% from the value given by BGPW. Other sources in the BGPW list have been extensively studied with VLBI and have been found to show flux density- as well as structural variability (e.g. 3C147; see discussion below). Both inadequate extrapolation and variability lead to internal inconsistencies of the flux densities in the calibrator list. These inconsistencies can lead not only to errors in absolute flux densities and measured source spectra, but also to spurious "variability" of the target sources, if the measurements at different epochs cannot be referred to the same calibrator.

To improve the situation and reduce the internal inconsistencies, we made new measurements of the sources in the BGPW list between 1989 and 1992. 17 sources were observed at λ = 21, 11, 6, 2.8, 1.3, 0.9 and 0.7 cm with the 100 m telescope of the Max-Planck-Institut für Radioastronomie, Bonn. Sections 2 and 3 describe the observations and data reduction. In Sect. 4 the flux density ratios of 3C286 and 3C295 are discussed; it is argued that both sources have not shown any measurable variability in the past 20 years. We then use the spectrum of 3C295 to link our results to the scale of BGPW. This leads to an updated internally consistent set of secondary calibrators, which is connected to the absolute flux density scale through the spectrum of 3C295 determined by BGPW.

2. Observations

The measurements were made with the 100 m telescope of the Max-Planck-Institut für Radioastronomie at Bonn, using different types of correlation receivers; the output of the left hand circularly polarized channel was taken whenever possible. Table 1 lists the wavelengths, exact frequencies and band widths, half power beam widths (HPBW), numbers of feeds, and mean system temperatures. At 1.3 cm a linearly polarized double-horn system was used in August 1989, but afterwards only a circularly polarized total power receiver was available.

For pointlike and slightly extended sources the telescope pointing offset was determined by an initial cross-scan through the nominal source position. A second cross-scan through the corrected position was then used to measure the flux density.

Send offprint requests to: M. Ott

Table 1. Receivers at the 100 m telescope used for this work. The bandwidth $\Delta\nu$ is given in col. 3

λ [cm]	ν [MHz]	$\Delta\nu$	θ_{HPBW}	feeds	T_{sys} [K]
21	1408	20	9.4′	1	45
11	2695	80	4.4′	1	80
6	4750	500	2.5′	2	60
2.8	10550	300	68″	2 (4)	50
1.3	23780	50-250	41″	2	30-60
1.3	22256	50-200	41″	1	30-60
0.9	32000	∼ 1000	28″	3	450
0.7	43200	500	22″	1	300

Table 2. Log of the observations

λ [cm]	ν [MHz]	date	Julian date 244...
21	1408	10 Feb 90	7933
		12 Feb 90	7935
11	2695	25 Jan 90	7917
		06 Oct 90	8171
6	4750	14 Mar 90	7965
2.8	10550	02 Jan 90	7894
		06 Jan 90	7898
1.3	22256	22 May 90	8034
		16 Jul 90	8089
		13 Nov 90	8209
		14 May 91	8391
		17 May 91	8394
		12 Nov 91	8573
	23780	08 Aug 89	7752
0.9	32000	11 Aug 91	8480
0.7	43200	25 Jun 90	8068
		05 Sep 91	8505
		05 Apr 91	8352
		14 May 92	8757

This procedure allowed us to correct for residual pointing offsets and therefore gives the most accurate results for strong sources, where thermal noise is not dominant. Each scan consisted of four or six subscans in elevation, followed by the same number of subscans in azimuth. Scanning in elevation and azimuth rather than right ascension and declination ensures that identical slices through the telescope beam pattern are used for all sources. Maps of the resolved sources were made by scanning a field centered on the source in rows separated by HPBW/2.

The sources were generally observed at elevations $> 30°$. A telescope gain curve (including atmospheric attenuation) was determined for each session from measurements of one source between 20° and 70° elevation. We observed mainly at night to get stable gains and a stable pointing.

Table 2 gives a summary of the observations, and Table 3 shows the source list, including the adopted average spatial extensions and references. For size correction factors see Sect. 3.

Table 3. Sources and their average extensions

sources	class	adopted exten. ["]	×	["]	ref.
0134+329 3C48	QSO	1.5	×	1.5	B,E,J
0223+617 W3(OH)	HII	2	×	6	D
0433+296 3C123	GAL	23	×	5	C,M
0538+498 3C147	QSO	1	×	1	A
0624−058 3C161	GAL	3	×	3	B
0915−119 3C218	GAL	47	×	15	2,B,I
0945+077 3C227	GAL	200	×	50	1,B
1100+772 3C249.1	QSO	15	×	15	2,F
1228+127 3C274 VirA	GAL	150	*to*	250	1,2
1328+307 3C286	QSO	1.5	×	1.5	K
1409+524 3C295	GAL	5	×	1	L
1458+717 3C309.1	QSO	1.5	×	1.5	H,K
1648+051 3C348	GAL	170	×	25	1
1717−009 3C353	GAL	210	×	60	1
1957+406 3C405 CygA	GAL	170	×	45	1
2037+422 DR21	HII	20	×	20	1
2105+420 NGC7027	PN	7	×	10	G

Classification:
QSO quasar GAL radio galaxy
PN planetary nebula HII H(II) Region

References for extensions:
1 maps with 100m telescope
2 deconvolution of cross-scans (100m telescope)
A Alef et al. 1990
B Baars et al. 1977 (BGPW)
C Branson et al. 1972
D Guilloteau et al. 1985
E Klein & Stelzried 1976
F Leahy et al. 1989
G Masson 1989
H Pearson et al. 1985
I Taylor et al. 1990
J Turegano & Klein 1980
K Van Breugel et al. 1984
L Wegner & Quirrenbach (VLA, priv. comm.)
M Riley & Pooley 1978

3. Data reduction

3.1. Cross-scans

In the first step of the data reduction, each subscan was examined, and those affected by interference or instrumental problems were deleted. Gaussians were fitted to individual subscans, and the fits for all subscans in a scanning direction (azimuth or elevation) were averaged. The peak values of the Gaussian fits were corrected for pointing offsets in both directions. Afterwards, the results of the two scanning directions were averaged. A telescope gain curve was determined for each observing run and applied to the data. In some cases, the data on the strongly polarized source 3C286 had to be corrected for a slight directional dependence of telescope and receiver feed to the intrinsic

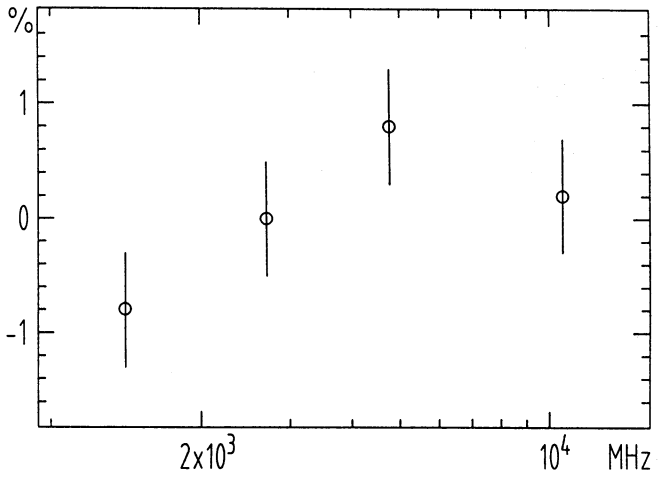

Fig. 1. Ratio of the flux densities of 3C286 to 3C295 compared to the value given by BGPW; deviation in percent

polarization of the source. The results of the individual scans on each source were then averaged for each epoch.

To correct for spatial extensions, we determined the HPBW of the telescope using the mean HPBW of the Gaussian fits to the point sources. The correction factor depends on the brightness distribution of the source. In case of a Gaussian brightness profile it is given by

$$C_g^2 = [1 + (\phi_S/\phi_B)^2][1 + (\theta_S/\theta_B)^2], \quad (1)$$

which results from the convolution of two Gaussians. Here S and B denote source and beam, and ϕ and θ the two axes of the elliptical Gaussian (azimuth and elevation).

For a disk-like distribution the correction factor is

$$C_d = \left[(1 - e^{-x^2})/x^2\right]^{-1} \text{ with } x = (4 \ln 2)^{1/2} * R/\theta_{\text{HPBW}} \quad (2)$$

(Ulich & Haas 1976; Ulich et al. 1980), where R is the angular radius of the disk (geometric mean of the axes) and θ_{HPBW} the beam width of the telescope. Equation 2 was applied to NGC7027, while Eq. 1 was applied to all other sources. For practical use we calculated mean correction factors to account for cross scans in varying directions across the sources. Dent (1972) derives a special correction factor for DR21. Within the errors, our correction factors are consistent with those of Dent. The size correction factors C_g and C_d are listed in Table 4.

Finally, as discussed in Sect. 4, our relative values were linked via scale factors to the absolute flux density scale using the BGPW spectrum of 3C295 (21 to 1.3 cm). For this purpose, the spectrum for 3C295 had to be extrapolated to 1.3 cm (see Table 6 in BGPW). The derived value of 0.84 Jy at 23780 MHz is consistent with the value of 0.56±0.11 Jy determined by Geldzahler & Witzel (1981) at 31.4 GHz and our value at 32 GHz. The flux densities at 7 mm were taken from Krichbaum et al. (1993), who calibrated with measurements of planets. The 9 mm data were scaled using NGC7027. Its flux density at 9 mm was determined from a fit to its thermal spectrum at 2.8, 1.3 and 0.7 cm (see Tables 4 and 6).

Table 4. Results; Columns are explained in Sec. 4.2.; "scale" in the rightmost column denotes that the flux density value was used for fixing the absolute scale at this frequency.

source	ν [MHz]	JD 244..	S [Jy]	ΔS [Jy]	N	C_g or C_d	diff. [%]
	1408	7933[1]	16.27	0.08	25	1.000	+2.5
3C48	2695	8171	9.49	0.05	18	1.000	+3.0
	4750	7965	5.72	0.03	2	1.000	+4.0
0134+329	10550	7894[2]	2.65	0.01	4	1.001	+6.3
	23780	7752	1.11	0.02	3	1.001	+7.8
W3(OH)	23780	7752	3.17	0.03	5	1.010	—
0223+617	43200	8352[3]	3.72	0.06	15	1.03	—
	1408	7933[1]	47.47	0.24	7	1.001	−2.0
3C123	2695	8171	27.62	0.14	6	1.003	−3.0
	4750	7965	16.56	0.08	3	1.009	−4.1
0433+296	10550	7894[2]	7.27	0.04	5	1.042	−9.7
	23780	7752	3.12	0.09	1	1.111	−9.5
	1408	7933[1]	21.86	0.11	4	1.000	−2.2
3C147	2695	8171	13.04	0.07	9	1.000	−4.2
	4750	7965	7.92	0.04	12	1.000	−5.3
0538+498	10550	7894[2]	3.68	0.02	5	1.000	−4.5
	23780	7752	1.70	0.02	2	1.001	+7.7
3C161	1408	7933[1]	18.58	0.09	7	1.000	−2.0
	2695	8171	11.13	0.06	5	1.000	−2.7
0624−058	4750	7965	6.75	0.03	3	1.000	−2.8
	10550	7894[2]	2.94	0.02	4	1.002	−6.3
3C218	1408	7933[1]	42.65	0.11	7	1.004	−0.4
	2695	8171	23.19	0.12	6	1.017	−2.2
0915−119	4750	7965	13.65	0.07	3	1.053	−3.6
	10550	7894[2]	6.53	0.04	4	1.245	−4.7
3C227	1408	7933[1]	7.61	0.04	7	1.048	+6.0
0945+077	2695	8171	4.39	0.02	8	1.208	+4.6
	4750	7965	2.96	0.10	1	M	+12.7
3C249.1	1408	7933[1]	2.28	0.01	6	1.001	−7.5
1100+772	2695	8171	1.33	0.01	4	1.003	−5.1
	4750	7965	0.82	0.01	2	1.010	+1.0
	1408	7933	203.0	6.0	1	M	−4.6
3C274	2695	7917[4]	121.7	2.1	2	M	−0.3
1228+127	4750	7965	77.3	2.0	1	M	+2.9
	10550	7898	40.2	1.6	1	M	+6.0

3.2. Error estimate for the cross-scans

It is straightforward to compute the uncertainties of the average relative flux densities: the error of the flux density of each scan results from the uncertainties in the Gaussian fits to the subscans and an error from the application of the gain curve. The mean value for each source at any epoch is given by the weighted average of individual scans; its error can therefore be calculated using standard error propagation formulae.

To get the final errors, the size correction factor and the scaling factor must be taken into account. The error in the size correction factor (C_g, eq. 1; C_d, eq. 2) is of order of a few percent; it results from uncertainties in the shape and extension of the source, and in the HPBW of the antenna. The errors in source extensions were estimated from maps in the literature (see Table 3) and range from 1″ to 20″. For the error of the HPBW, a value of 2″ was used.

The measured flux densities can be affected by confusing sources within the beam. The rms confusion for the 100m antenna is estimated as 0.03 Jy at 1408 MHz, or 0.005 Jy at 2695 MHz and is negligible at higher frequencies. We have not added these confusion errors to the errors of measurement quoted in Tables 4 and 6.

To link our results to an absolute scale, we calculated scaling factors to the spectrum of 3C295 in BGPW (cf. Table 5 in BGPW). The formal errors of these factors contain the uncertainty of our data and that from BGPW for 3C295. No errors are available for the relative flux densities listed by BGPW; as an approximation we apply the errors of our own measurements instead. The final errors listed in Table 4 were obtained by adding

Table 4. (continued)

source	ν [MHz]	JD 244..	S [Jy]	ΔS [Jy]	N	C_g or C_d	diff. [%]
	1408	7933[1]	14.68	0.07	6	1.000	−0.8
3C286	2695	8171	10.52	0.05	8	1.000	0.0
	4750	7965	7.60	0.04	2	1.000	+0.8
1328+307	10550	7894[2]	4.45	0.02	15	1.001	+0.2
	22256	8034[5]	2.38	0.02	10	1.001	−6.5
	32000	8480	2.04	0.07	5	1.003	—
	43200	8352	1.86	0.26	3	1.005	—
	1408	7933[1]	22.22	0.11	7	1.000	scale
3C295	2695	8171	12.24	0.06	13	1.000	"
	4750	7965	6.74	0.03	2	1.000	"
1409+524	10550	7894[2]	2.58	0.01	11	1.002	"
	22256	8034[6]	0.92	0.01	12	1.005	"
	23780	7752	0.84	0.01	35	1.005	scale
	32000	8480	0.57	0.03	3	1.011	—
	1408	7933[1]	7.48	0.04	5	1.000	—
3C309.1	2695	8171	4.72	0.02	6	1.000	—
	4750	7965	3.20	0.02	3	1.000	—
1458+718	10550	7894[2]	1.82	0.01	6	1.001	—
	22256	8034[7]	1.00	0.02	7	1.001	—
	23780	7752	0.96	0.01	5	1.001	—
	32000	8480	0.76	0.15	1	1.004	—
3C348	1408	7933[1]	46.73	0.23	8	1.029	+4.5
	2695	8171	23.37	0.29	3	1.126	+3.4
1648+051	4750	7965	13.11	0.40	1	M	+5.3
	10550	7898	4.83	0.20	1	M	−10.2
3C353	1408	7933[1]	56.25	0.28	5	1.056	−1.4
	2695	8171	34.26	0.24	1	1.244	−2.2
1717−009	4750	7965	23.49	0.75	1	M	+6.0
	10550	7898	10.71	0.40	1	M	−3.0
Cyg A	4750	7965	403.4	12.0	1	M	−4.4
1957+406	10550	7898	115.7	4.0	1	M	+19.2
	2695	8171	14.99	0.07	3	1.005	—
	4750	7965	19.07	0.80	1	M	—
DR21		7965	19.10	0.10	2	1.018	—
2037+422	10550	7894[2]	20.02	0.08	5	1.087	−4.0
	22256	8089	17.04	0.69	1	1.238	−10.5
	1408	7933	1.34	0.01	9	1.000	−1.4
		7935	1.37	0.01	6	1.000	+0.8
NGC7027	2695	8171	3.62	0.02	21	1.000	+3.4
	4750	7965	5.47	0.03	5	1.001	∼0.0
2105+420	10550	7894	6.13	0.04	4	1.005	−4.8
		7898	6.10	0.05	2	1.005	−5.3
	22256	8209	5.64	0.11	3	1.015	−3.8
		8391	5.39	0.05	2	1.015	−8.0
		8573	5.70	0.08	2	1.015	−2.7
	23780	7752	5.39	0.04	29	1.015	−9.2
	32000	8480	5.23	0.19	5	1.031	scale
	43200	8086	5.20	0.81	1	1.043	—
		8352	5.39	0.40	8	1.051	—
		8505	4.95	0.32	12	1.051	—
		8757	5.12	0.28	9	1.051	—

1) average of epoch 2447933 and 2447935.
2) average of epoch 2447894 and 2447898.
3) average of epoch 2448352 and 2448575.
4) average of epoch 2447917 and 2448171.
5) average of epoch 2448034, 2448089 and 2448209.
6) average of epoch 2448034, 2448089, 2448209, 2448394, and 2448573.
7) average of epoch 2448034, 2448089, and 2448391.

quadratically the errors associated with the flux density measurements, the correction factors, and the scaling procedure. In several cases the statistical errors are below 0.5 percent; in these cases we give errors of 0.5%.

3.3. Maps

For the (more than marginally) resolved sources maps were made and reduced with the standard software of the MPIfR. The integral of the flux density in each map was calculated and calibrated with maps of the point source 3C286 obtained in the same way. Flux densities derived from maps are denoted by 'M' in Table 4.

The flux density errors resulting from maps are composed of those due to the integration method, polarization (in the case of 3C286 at 2.8 cm) and the gain curve of the telescope. The inaccuracy of the integral method was estimated by varying parameters during data processing. It lies in the range of 2% to 4%; the errors associated with gain and polarization corrections are considerably smaller ($\sim$ 1% and $\leq$ 1%, respectively). The conversion to the absolute scale was treated in the same way as for the unresolved and the marginally resolved sources.

4. The updated calibrator list

4.1. Non-variable sources

To investigate the variability of the sources in our list, we have calculated the ratios of flux densities (S_x/S_y) for all source pairs x, y. These ratios then were compared to those from BGPW:

$$Q = \left(S_x/S_y\right)_{\rm new} / \left(S_x/S_y\right)_{\rm BGPW}, \quad P = (Q-1) * 100 \quad , \quad (3)$$

i.e. P denotes the percentage change of the ratio compared to the BGPW value. We find that within the range 2.8 cm $\leq \lambda \leq$ 21 cm, the flux density ratios of 3C286 and 3C295 have remained constant to within 2% (see Fig. 1).

The radio galaxy 3C295 shows two lobes of almost equal brightness at a separation of 4″. The lobes have diameters of order 5 kpc each (Laing 1981; Baum et al. 1988). A VLA-map (2 cm, A configuration) by Baum et al. (1988) shows evidence for core emission at the level of about 0.4% of the total flux density at 2 cm (1.6 Jy). Therefor the flux density of 3C295 is expected to be constant to within 1% for hundreds to thousands of years. The quasar 3C286 shows the flattest synchrotron spectrum ($\alpha_{1.3}^{21} = -0.65$; $S_\nu \propto \nu^{+\alpha}$) of all extragalactic sources in our list. Its polarization in the range of 21 to 1.3 cm is about 11% (cf. BGPW; Aliakberov et al. 1985).

It is very unlikely that these two sources should have undergone large flux density variations which contrive to give constant ratios of S_{3C286}/S_{3C295}. This argument, together with the one above, based on the structure of 3C295, leads us to conclude that neither 3C295 nor 3C286 have varied by more than $\sim$ 1% since 1976 (for 2.8 cm $\leq \lambda \leq$ 21 cm). Therefore these sources can be used to link our relative flux density measurements to the absolute scale of BGPW.

From Fig. 1 we estimate that the internal calibration error for our new consistent list is $\sim$ 2% in the range 2.8 cm $\leq \lambda \leq$ 21 cm. The absolute scale of BGPW was estimated to be accurate to $\sim$ 5% by the authors.

The situation is more complicated at 1.3 cm. As listed in Table 4, the flux density of 3C286, compared to that of 3C295, appears to be 6.5% lower at this wavelength than expected from BGPW. The BGPW values at 1.3 cm for either source might simply be off by a few percent, since they are based on extrapolations of the source spectra. Alternatively, one of the sources (more likely 3C286 because of its higher compactness) might have varied at high frequencies. For 3C286 there is some indication for a core component becoming visible in the spectrum below $\lambda \leq$1 mm. In any case, the uncertainty of the absolute flux density scale at 1.3 cm is probably about 10%.

4.2. Results and discussion of individual sources

In Table 4 we present our final results (Cols. 4 and 5). The listed mean flux densities were obtained from weighted averages of the values from the individual epochs. These values contain the

Table 5. New spectral fits for calibrator sources

$\log S$ [Jy] = a + b * $\log \nu$ [MHz] + c * $\log^2 \nu$ [MHz]					
source	range [MHz] from	to	a	b	c
3C48	1408	23780	2.465	−0.004	−0.1251
3C123	1408	23780	2.525	+0.246	−0.1638
3C147	1408	23780	2.806	-0.140	−0.1031
3C161	1408	10550	1.250	+0.726	−0.2286
3C218	1408	10550	4.729	−1.025	+0.0130
3C227	1408	4750	6.757	−2.801	+0.2969
3C249.1	1408	4750	2.537	−0.565	−0.0404
VirA	1408	10550	4.484	−0.603	−0.0280
3C286	1408	43200	0.956	+0.584	−0.1644
3C295	1408	32000	1.490	+0.756	−0.2545
3C309.1	1408	32000	2.617	−0.437	−0.0373
3C348	1408	10550	3.852	−0.361	−0.1053
3C353	1408	10550	3.148	−0.157	−0.0911
CygA	4750	10550	8.360	−1.565	—
NGC7027	10550	43200	1.322	−0.134	—

NGC7027 flux densities reduced to epoch JD = 2448171. Fit to points at 2.8, 1.3 and 0.7 cm.
DR21 Complexity of spectrum allows no overall fit.

size correction factors given in Col. 7 (C_g or C_d). An M in Col. 7 denotes that the source was mapped. Col. 6 lists the number of scans, and Col. 8 shows the percentage difference P of the flux densities compared to the values listed by BGPW. Fig. 2 and 3 show the spectra. Second order polynomials in $\log S$ were fitted to the data points as a function of $\log \nu$. The coefficients of these fits are presented in Table 5.

The values listed in Table 4 suggest significant variability of several sources. However, most of the differences compared to BGPW lie within ~5%. In most cases we believe that we have more accurate results than BGPW. When the observations of BGPW were carried out (around 1975), source extensions were not known as well as today. Extensions were often derived from deconvolution, since high resolution maps were not available. Additionally, BGPW compiled flux densities from older measurements; the inhomogenity of their data set makes an assessment of the errors of individual values extremely difficult. In particular, BGPW may have underestimated the uncertainties at 2.8 cm, which might be as large as 10% for data obtained in the early seventies. Nevertheless, our results seem to show tendencies of spectral changes in some cases. We discuss the sources in the following:

The quasar 3C48 appears to have become brighter, especially at shorter wavelengths. The differences with respect to the BGPW flux densities are 2.5% at 21 cm, and 8% at 1.3 cm. These changes are consistent with activity in the core (Wilkinson et al. 1990).

The quasar 3C147 appears to be fainter by 2-5% between 21 and 2.8 cm. At 1.3 cm there seems to be a strong increase in brightness (7-8%), which could be explained as follows: (a) the extrapolated BGPW value underestimated the 1.3 cm flux density, or (b) a real increase at high frequencies may origin from the ejection of a new VLBI component. VLBI observations show apparent superluminal motion of 1.3 c on the milliarcsecond scale (H_0 =100 km s^{-1} Mpc^{-1}; q_0 =0.5) and an increase of 2.5% in the core flux density at 5 GHz between epochs 1981.3 to 1984.8 (Alef et al. 1990). Simon et al. (1983) observed an increase in flux density from 0.9 Jy in 1975 to 2.0 Jy in 1981 at 329 MHz and explain it by structural variability. The use of 3C48 or 3C147 as calibrators requires frequent checks with 3C286 or 3C295, if accuracies better than ~ 5% are desired.

The radio galaxies 3C123, 3C161 and 3C218 show lower flux densities than given by BGPW at all frequencies. The apparent fading of these sources might partly be due to an overcorrection for the extension by BGPW. For 3C123, the difference sums up to 9% at 2.8 cm. The value at 1.3 cm is rather uncertain, as it results from only one scan measured with the linearly polarized system. BGPW give a polarization of 2% for this source. Our results for 3C161 and 3C218 between 21 and 6 cm lie within the error range of BGPW, but are more accurate. However, a study of 3C161 by Andrew et al. (1978) shows variations of ~ 10% at 2.8 cm and 4.5 cm (1966 to 1973, accuracy 5%). These sources are acceptable as calibrators, but their flux densities should occasionally be checked against 3C286 and 3C295, if accuracies better than ~ 5% are desired.

The radio galaxy 3C274 (Vir A) was mapped at λ = 21, 11, 6 and 2.8 cm. Within the error range of BGPW, the results show a tendency towards a flatter spectrum which could be due to core activity. The increase of flux density for the radio galaxy 3C227 could likewise be explained by an active nucleus. For the spectra of the radio galaxies 3C348 and 3C353 we get somewhat stronger spectral curvatures than BGPW. Because of their spatial extensions, the flux densities of these four sources are difficult to measure with the 100 m telescope, and they are certainly not usable as calibrators with this instrument. On the other hand, they are good secondary standards for smaller telescopes because of their strength, if an accuracy of ~ 5% is sufficient.

The quasar 3C249.1 has been used as a calibrator mainly because of its high declination (δ = 77°). However, its spectrum appears to be flatter than expected from BGPW. The source is comparatively weak which may have induced additional errors in earlier data. We have tried to use the quasar 3C309.1 (1458+71, $\alpha_{2.8}^{21}$=-0.7) to calibrate the observations of high-declination sources instead, but on time scales of several years theissource is known to vary (Klein and Stelzried 1976; Andrew et al. 1978). Comparing our flux density at 2.8 cm to that of Kühr et al. (1981), we find a decrease of 7%. This decrease could be traced back to variations in the flat spectrum core (α_2^6 = −0.4; Van Breugel et al. 1984). Both 3C249.1 and 3C309.1 can be used for calibration, provided their flux densities are checked from time to time.

The planetary nebula NGC 7027, because of its brightness at short wavelengths, is an important calibrator. However, it

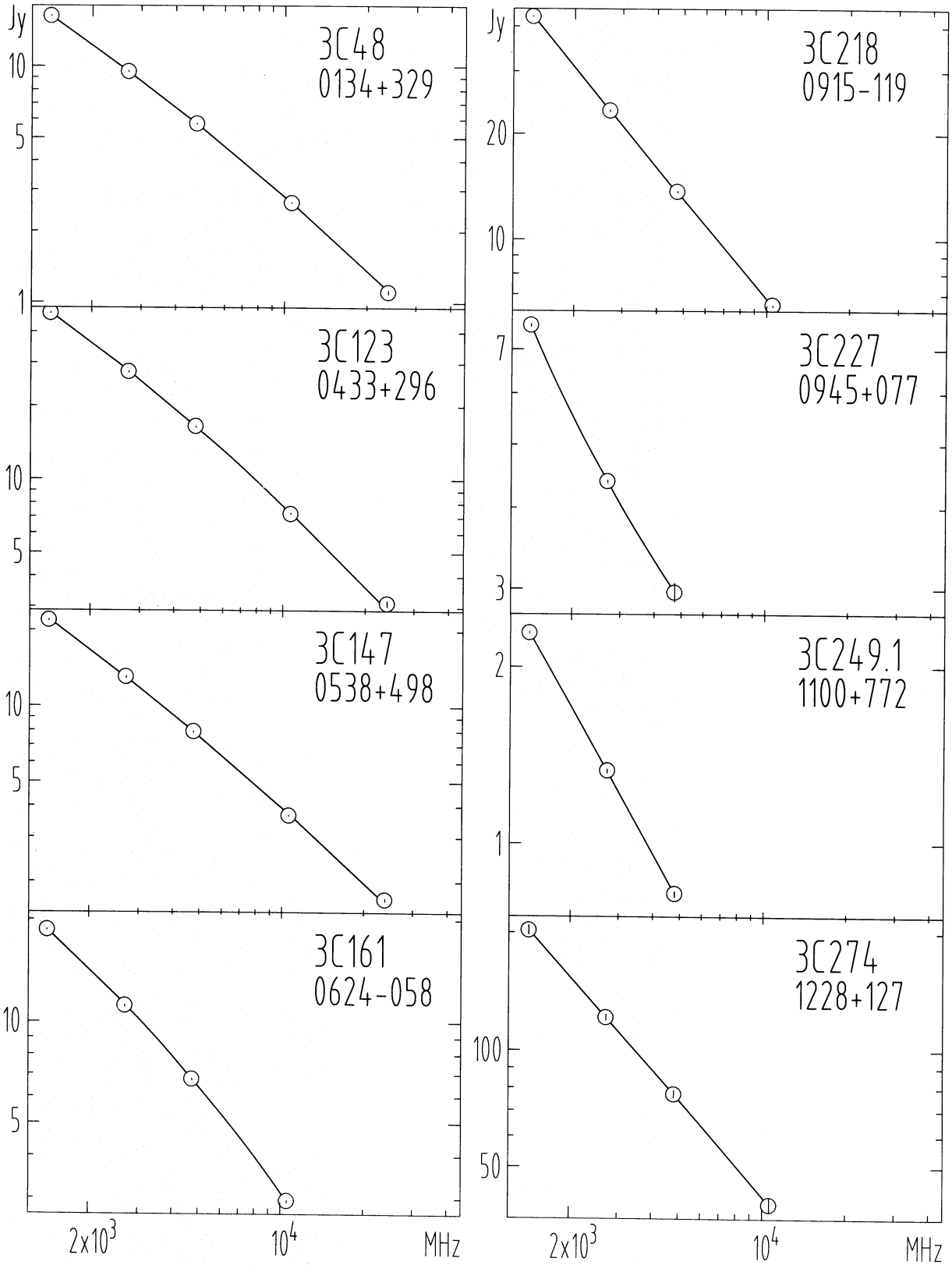

Fig. 2. a Spectra from Table 4, fits as from Table 5

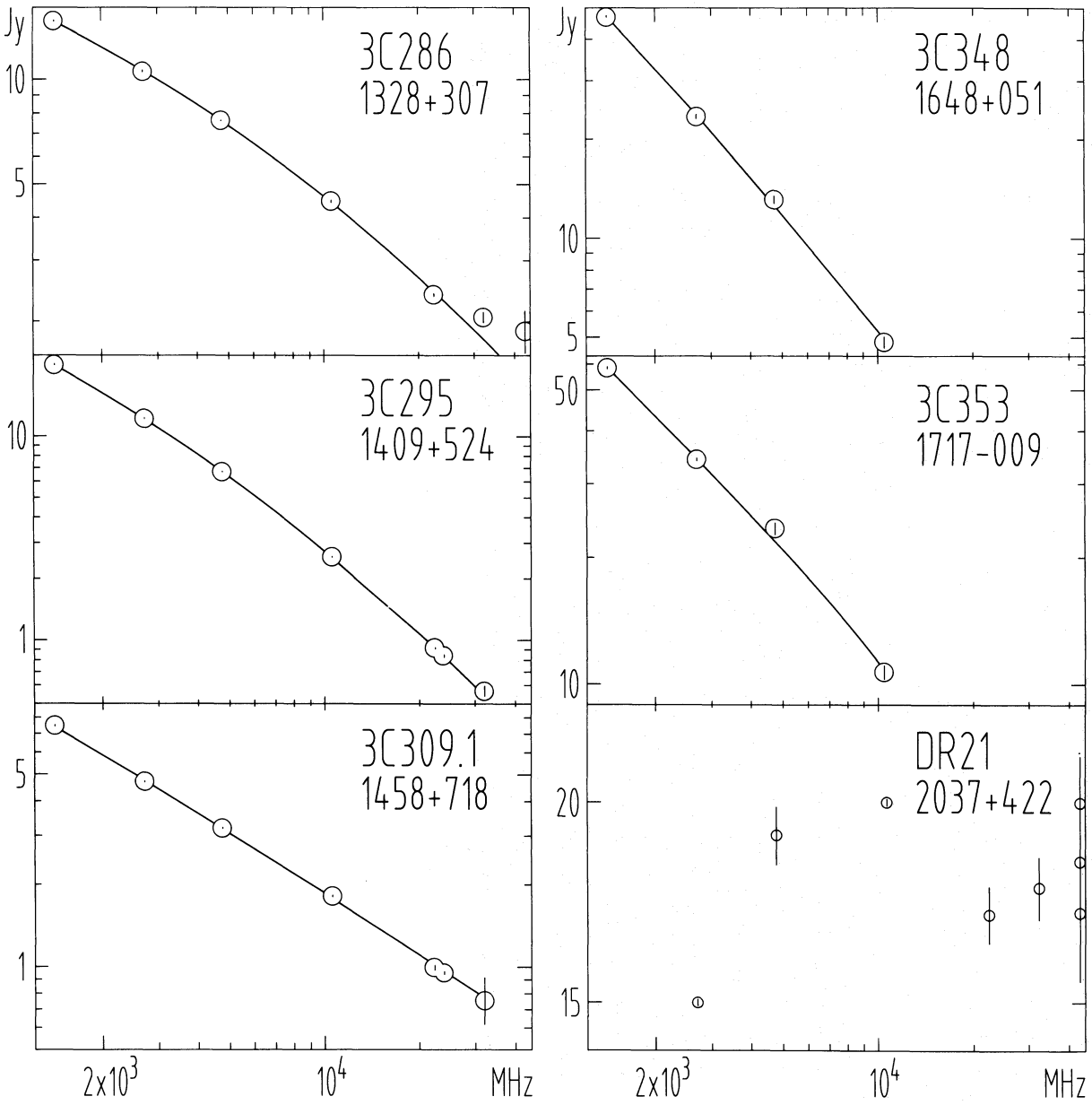

Fig. 2. b Spectra from Table 4, fits as from Table 5

shows a pronounced decrease in its flux density at short wavelengths ($\lambda < 6$ cm) and a possible increase in the flux densities at wavelengths longer than 6 cm. It was tried to account for these changes using a model of an expanding planetary nebula which involves an ellipsoidal shell (Masson 1989) of thickness $\Delta r/r = 0.342$, an axial ratio of 2.6, an inclination of the major axis to the line of sight of 30 degrees and an electron temperature in the shell of 14500 K. A model was fitted to both the BGPW data and the present data, keeping the geometry constant (Pauliny-Toth, priv. comm.). In doing this, we have reduced the present spectrum of NGC 7027 to a mean epoch JD=2448171 (Oct. 6th, 1990, or 1990.77). To calculate the annual change of its flux densities, we adopted the epoch JD=2442873 (Apr. 4, 1976, or 1976.26) for the values given by BGPW. In Table 6, we list the averaged flux densities (from Table 4) reduced to epoch JD=2448171, together with their annual changes. The annual changes derived from fits of the above model to the BGPW and the present data are of the same order as the values listed in Table 6 with an exception: at 21 cm where the model results in an annual increase of flux density of 0.7 percent. Fig. 3a shows the spectrum obtained from the data quoted in Table 4, and Fig. 3b shows the reduced spectrum obtained from Table 6. At frequencies above 10 GHz, a simple power law can be used to represent the spectrum of NGC 7027. Its parameters (Table 5, obtained from flux densities at 2.8, 1.3 and 0.7 cm) were used to calculate the flux density at 0.9 cm, and used to scale the measurements of other sources at this wavelength.

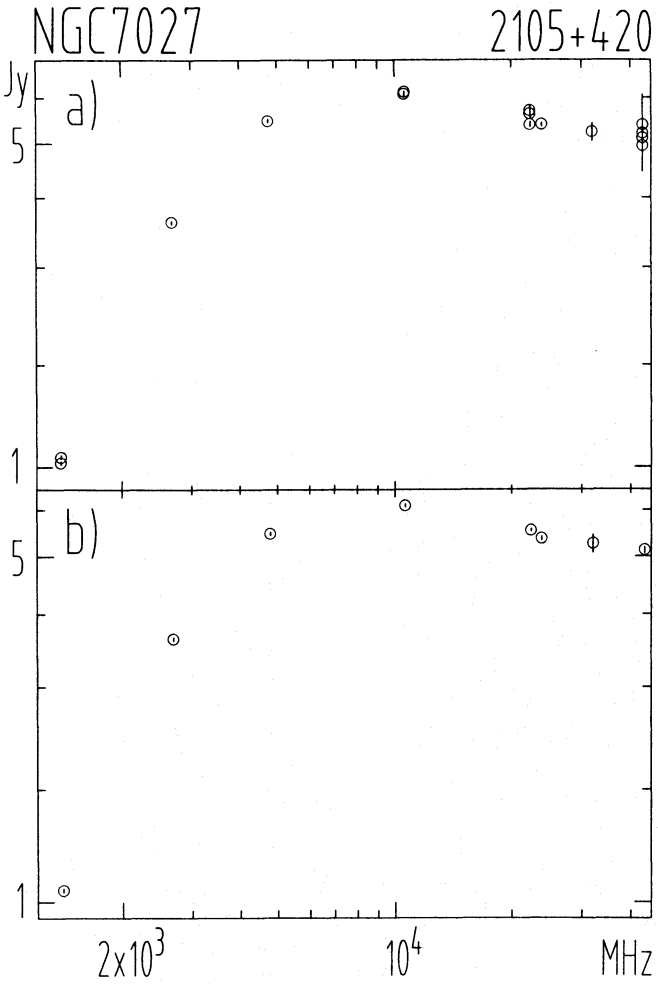

Fig. 3a and b. NGC 7027. **a** Spectrum from Table 4, and **b** reduced spectrum for epoch JD=2448171 as from Table 6 (see text)

Two HII regions in the galactic plane are frequently used as calibrators, namely W3(OH) and DR21. However, for both sources, accurate measurements are made difficult due to confusion by several surrounding features at longer wavelengths and internal structure resolved at shorter wavelengths. For W3(OH) we only could determine flux densities at 1.3 and 0.7 cm. Our measurements of DR21 seem to indicate a slightly lower flux density at short wavelengths than given by BGPW. The results at 0.9 and 0.7 cm are consistent with values expected from a thermal spectrum, but the size correction factor at the 100 m telescope is too large for giving reliable results.

Crane (1991) observed NGC7027 along with 3C48, 3C147 and 3C286 at 22460.1 MHz with the VLA in December 1989. The flux density ratios of 3C286, NGC7027 and 3C147 agree with our ratios within the errors. The ratios for 3C48 differ by at least 3σ, however. This is consistent with our conclusion that core variability is important at high frequencies in 3C48.

Table 6. NGC7027; average flux densities reduced to epoch JD= 2448171 (Oct 9, 1990). Size correction cf. Table 4.

ν [MHz]	S [Jy]	ΔS [Jy]	N	annual change [%]
1408	1.34	0.01	15	± 0.0
2695	3.62	0.02	21	+0.24
4750	5.47	0.03	5	± 0.0
10550	6.10	0.03	6	−0.36
22256	5.53	0.03	7	−0.5
23780	5.36	0.04	29	−0.5
32000	5.25	0.19	5	−0.6
43200	5.13	0.06	30	−0.6

5. Conclusion

The calibrator list of Baars et al. (1977, BGPW) has been the widely accepted standard for flux density calibration during the last fifteen years. However, considerably higher accuracies for relative flux densities are easily obtained with modern instruments. We have made new measurements of the BGPW sources to reduce the internal inconsistencies in this set of secondary calibrators. Our assessment of individual calibrators, based on new relative flux density measurements in the range 0.9 cm $\leq \lambda \leq$ 21 cm can be summarized as follows:

- 3C295 and 3C286 have not shown variability in excess of $\sim$ 1% during the last decades. At least for 3C295, a very low degree of variability is also expected on morphological grounds. This suggests the use of these sources as the main standards for single dish telescopes. 3C286 is also compact enough to serve as an interferometer standard. The only caveat is its high degree of polarization.
- NGC7027 is a suitable calibrator, especially at high frequencies, if the source size at short wavelengths and the secular changes of its spectrum are taken into account.
- 3C48, 3C123, 3C147, 3C161, 3C249.1, and 3C309.1, are also suitable as flux density calibrators. However, some of these sources show variability on the order of a few percent. Their flux densities should be compared regularly to 3C295 and 3C286. These sources are almost pointlike; they can be used as calibrators at a 100 m telescope.
- 3C218, 3C227, 3C274, 3C348, 3C353, and DR21 are more extended, and our measurements are somewhat less reliable than for the less extended sources. There are indications of variability at the level of 5 to 10%.
- The accuracy of the absolute flux density scale has been estimated by BGPW to be of the order 5% in the range 2 cm $\leq \lambda \leq$ 70 cm. It is probably about 10% at 1.3 cm, and possibly somewhat worse at 0.9 and 0.7 cm.

Acknowledgements. It is a pleasure to thank the referee J.M. Riley who suggested some improvements in this paper. We acknowledge helpful discussions with W.J. Altenhoff, I.I.K. Pauliny-Toth and L. Sage. The observations would not have been possible without the support of the staff at the 100 m telescope. A.Q. thanks the Alexander von Humboldt Foundation for support through a Feodor Lynen Fellowship.

References

Alef W., Preuss E., Kellermann K.I., 1990, in Compact Steep-Spectrum & GHz-Peaked Spectrum Radio Sources, Fanti et al. (eds.), Proceedings, Dwingeloo Workshop June 18-19 1990, printed by Istitutio di Radioastronomia, Bologna

Aliakberov K.D., Mingaliev M.G., Naugol'naya M.N., Trushkin S.A., Shapirova L.M., Yusupova S.N., 1985, Izvestiya Spetsial'noi Astrofizicheskoi Observatorii 19, 60

Andrew B.H., MacLeod J.M., Harvey G.A., Medd W.J., 1978, AJ 83, 863

Baars J.W.M., Genzel R., Pauliny-Toth I.I.K., Witzel A., 1977, A&A 61, 99 (BGPW)

Baum S.A., Heckman T.M., Bridle A.H., Van Breugel W.J.M., Miley G.K., 1988, ApJS, 86, 643

Branson N.J.B.A., Elsmore B., Pooley G.G., Ryle M., 1972, MNRAS 156, 377

Crane P., 1991, VLA Test Memorandum No. 159, Socorro

Dent W.A., 1972, ApJ, 177, 93

Findlay J.W., 1966, ARA&A 4, 77

Geldzahler B.J., Witzel A., 1981 AJ 86, 1036

Guilloteau S., Baudry A., Walmsley C.M., 1985, A&A 153, 179

Kellermann K.I., Pauliny-Toth I.I.K., Williams P.J.S., 1969, ApJ 157, 1 (KPW)

Klein M.J., Stelzried C.T., 1976, AJ 81, 1078

Krichbaum T.P., Witzel A., Graham D.A., Standke K.J., 1993, A&A 275, 375

Kühr H., Pauliny-Toth I.I.K., Witzel A., Nauber U., 1981, A&AS 45, 367

Ivanov V.P., Stankevich K.S., 1989, SvA Lett. 33, 15

Laing R.A., 1981, MNRAS 195, 261

Leahy J.P., Muxlow T.W.B., Stephens P.W., 1989, MNRAS 239, 401

Masson C.R., 1989, ApJ 336, 294

Moiseev I.G., Nesterov N.S., 1987, Bull. Crim. Ap. Obs. 73, 137

Pearson T.J., Readhead A.C.S., Wilkinson P.N., 1980, ApJ 236, 714

Pearson,T.J., Perley R.A., Readhead A.C.S., 1985, AJ 90, 738

Riley J.M., 1988, MNRAS 233, 225

Riley J.M., Pooley G.G., 1978, MNRAS 183, 245

Simon R.S., Readhead A.C.S., Moffet A.T., Wilkinson P.N., Anderson B., 1980, ApJ 236, 707

Simon R.S., Readhead A.C.S., Wilkinson P.N., Allen B., Burke B.F., 1983, Nat 302, 487

Taylor G.B., Perley R.A., Inoue M., Kato T., Tabara H., Aizu K., 1990, ApJ 360, 41

Turegano J.A., Klein M.J., 1980, A&A 86, 46

Ulich B.L., Haas R.W., 1976, ApJS 30, 247

Ulich B.L., Davis J.H., Rhodes P.J., Hollis J.M., 1980, IEEE Trans. Ants. and Prop. AP-28, 367

Van Breugel W., Miley G., Heckman T., 1984, AJ 89, 5

Véron M.P., Véron P., Witzel A., 1974, A&AS 13, 1

Wilkinson P.N., Tzoumis A.K., Akujor C.E., et al. , 1990, in: "Parsec-Scale Radio Jets", ed. J.A. Zensus and T.J. Pearson, Cambridge University Press, p. 152

This article was processed by the author using Springer-Verlag LaTeX A&A style file version 3.